Electrochimica Acta 263 (2018) 94–101

Contents lists available at ScienceDirect

Electrochimica Acta

journal homepage: www.elsevier.com/locate/electacta

3D hierarchical CMF/$MoSe_2$ composite foam as highly efficient electrocatalyst for hydrogen evolution

Yunpeng Huang [a], Fen Cui [b], Yan Zhao [a], Jiabiao Lian [a], Jian Bao [a], Tianxi Liu [c, **], Huaming Li [a, b, *]

[a] Institute for Energy Research, Jiangsu University, Zhenjiang, 212013, PR China
[b] School of Chemistry and Chemical Engineering, Jiangsu University, Zhenjiang, 212013, PR China
[c] State Key Laboratory for Modification of Chemical Fibers and Polymer Materials, College of Materials Science and Engineering, Donghua University, Shanghai 201620, PR China

ARTICLE INFO

Article history:
Received 4 September 2017
Received in revised form
12 December 2017
Accepted 3 January 2018
Available online 3 January 2018

Keywords:
3D flexible electrocatalyst
Hydrogen evolution
Melamine foam
Hierarchical composite foam

ABSTRACT

Exploration of high-performance Pt-free electrochemical catalysts for hydrogen evolution reaction (HER) mainly depends on the catalyst design and system construction. Here, a unique flexible HER catalyst of few-layered $MoSe_2$ nanosheets perpendicularly grown on 3D elastic carbonized melamine foam (CMF) is fabricated through a solvothermal reaction. The rationally designed 3D hierarchical CMF/$MoSe_2$ composite foam with conductive 3D networks and fully exposed $MoSe_2$ active edges can provide efficient and rapid pathways for ion and electron transport, thus delivering largely enhanced HER catalytic performance with a low onset potential (−0.071 V vs. RHE), small tafel slop (49.3 mV dec^{-1}), as well as excellent long-term stability. This research may pave the way for the development of flexible, lightweight, and low-cost catalysts for high-performance HER.

1. Introduction

With the growing concerns about the energy shortage and severe environmental contamination, global efforts have devoted into the exploration of renewable-energy sources as feasible alternatives to replacing conventional fossil fuels [1–4]. Owning to its zero carbon footprints and high energy density, hydrogen is widely regarded as promising clean energy carrier to satisfy the increasing energy demands [5,6]. Among the hydrogen production technologies, water electrolysis with electrocatalysts boosted hydrogen evolution reaction (HER) is the most promising and efficient approach for the future hydrogen mass production [7–9]. Therefore, electrocatalysts with high activity and low HER overpotential are particularly essential to promote the sluggish HER kinetics. Generally, noble metals, such as platinum (Pt), possess outstanding HER activity with zero HER overpotentials, howerver, their wide applications are greatly hindered by the high cost and scarcity [10,11]. Developing efficient noble metal-free HER electrocatalysts with low cost and environmental benignity has thus captured extensive research attention.

Up to now, a variety of earth-abundant HER catalysts, such as metal chalcogenides [12–14], oxides [15], hydroxides [16,17], phosphides [18–20], nitrides [21,22] and carbides [23,24], have been reported and received massive interests. Among these materials, transition metal dichalcogenides (TMDs) are considered as one type of the most attractive HER catalyst due to their tunable band structure and low intrinsic electrical resistivity that could promote charge transfer during electrochemical reaction [25,26]. As one member of TMDs, $MoSe_2$ is broadly recognized as excellent catalyst for HER because of its more metallic nature with respect to MoS_2 [27–29]. Both theoretical calculation and experimental studies revealed that the Gibbs free energy of hydrogen adsorption on $MoSe_2$ active sites is lower than that of MoS_2 [30], leading to the superior electrochemical activity of $MoSe_2$. Despite all the advantages, $MoSe_2$ always suffers from two severe drawbacks: (1) limited distribution of available electrochemical active sites, (2) sluggish reaction kinetics stemmed from the relatively low electrical conductivity of $MoSe_2$ [31]. Therefore, the catalytic performance of $MoSe_2$ still needs to be improved to compete with commercial Pt-

* Corresponding author. Institute for Energy Research, Jiangsu University, Zhenjiang, 212013, PR China.
** Corresponding author. State Key Laboratory for Modification of Chemical Fibers and Polymer Materials, College of Materials Science and Engineering, Donghua University, Shanghai, 201620, PR China.
E-mail addresses: txliu@dhu.edu.cn (T. Liu), lhm@ujs.edu.cn (H. Li).

https://doi.org/10.1016/j.electacta.2018.01.016
0013-4686/

based catalysts. To solve these problems, the most common strategy is to coating and nanostructuring with various conductive substrates (e.g., reduced graphene oxides [32,33], carbon nanotubes [34], carbon fiber cloth [35], Mo thin film [36]), thus improving the specific surface area and charge transfer efficiency of $MoSe_2$ catalysts. Nevertheless, the HER performance of these composites still need further improvement, and the powder state or fragility of most of the aforementioned catalysts also greatly hinders their practical applications.

Recently, porous three dimensional (3D) electrodes have attracted much attention due to their 3D interconnected networks and multi-dimensional porosity, thus affording fast charge and mass transfer through numerous electron/ion pathways during electrochemical process. Additionally, self-supported 3D electrodes are much easier to be processed and applied in practical circumstances than conventional materials. To date, largely enhanced performance has been achieved by growing electroactive materials on different porous 3D electrodes, such as 3D graphene aerogels/foams [37–39], 3D CNT aerogels [40], nickel foam [3], stainless steel mesh [41], and carbonaceous 3D foams [42]. However, graphene and CNT foams are unstable because of their poor mechanical strength, the structuring and interconnecting of building blocks are always hard to control [43]. As for metal networks, their applications are impeded by the rigid nature and weak flexibility. Recently, it was demonstrated that 3D interconnected carbon foams can be fabricated through direct carbonization of commercially available melamine foam [44–46]. Except the facile preparation and excellent mechanical properties of the carbon foams, enhanced electrochemical performance also can be achieved via the hybridization of electroactive materials with porous carbon foams.

Herein, we focus on the development of a new type of free-standing and compressive 3D carbon-backboned composite foam as high-performance HER electrocatalyst. The carbonized melamine foam (CMF) with 3D interconnected networks and macrospores is first prepared through high temperature carbonization, perpendicularly oriented few-layer $MoSe_2$ nanosheets are then successfully grown on CMF frameworks by a versatile solvothermal reaction. The 3D interconnected carbon structure not only direct the uniform growth of $MoSe_2$ nanosheets, thus greatly increase the exposed active edges of $MoSe_2$, the carbonaceous networks also serve as conducting backbone to promote the charge transfer. This rationally designed 3D CMF/$MoSe_2$ electrocatalyst manifests significantly enhanced electrochemical activity towards HER with a low onset potential (−0.071 V vs. RHE) and smaller Tafel slop (49.3 mV dec^{-1}).

2. Experimental

2.1. Materials

The melamine foam (MF) used in the experiments was obtained from SINOYQX (Sichuan, China). Na_2MoO_4 (99.99%), hydrazine hydrate ($N_2H_4\cdot H_2O$, 50 wt% in water), and Selenium powder (Se, 99.99%) were purchased from Sinopharm Chemical Reagent Co. Ltd. Pt/C catalyst (20 wt % platinum on carbon black) was obtained from Alfa Aesar. All other reagents were bought from Sinopharm Chemical Reagent Co. Ltd. Deionized (DI) water was used throughout the experiments.

2.2. Preparation of CMF/$MoSe_2$

The preparation method of 3D CMF/$MoSe_2$ composite foam is schematically depicted in Scheme 1. In a typical experiment, MF was carefully tailored into thin strips with the size about $50 \times 15 \times 2\ mm^3$, after thoroughly rinsing with ethanol and acetone under ultrasonication for 30 min, dried MF strips were carbonized in a tubular furnace under N_2 atmosphere at a heating rate of 10 °C min^{-1} up to 800 °C and held for 2 h. After cooling to room temperature, obtained CMF was immersed into HNO_3 solution for 1 h to remove any impurities, then washed with DI water for several times.

For the solvothermal reaction, a 3 mg mL^{-1} Se–$N_2H_4\cdot H_2O$ solution was first prepared in a flask by dissolving certain amount of Se powder into $N_2H_4\cdot H_2O$ solution under 80 °C water bath at magnetic stirring. Afterwards, 10 mL as-prepared dark-red Se–$N_2H_4\cdot H_2O$ solution was transferred into a 40 mL Teflon-lined autoclave, then stoichiometric amount of Na_2Mo_4 in 10 mL *N,N*-dimethylformamide (DMF) was added into the above solution to yield the mixture with a Mo:Se molar ratio of 1:2. A piece of CMF was then added to the mixed solution and allowed the autoclave heating in an oven at 180 °C for 12 h. After cooling to room temperature, self-standing CMF/$MoSe_2$ composite foam was withdrawn and rinsed gently with DI water for 3 times. After drying overnight at 80 °C, crystalized CMF/$MoSe_2$ composite foam was finally obtained after treating at 450 °C under N_2 atmosphere with a heating speed of 5 °C min^{-1} for 2 h. For comparison, pure $MoSe_2$ was also synthesized in a similar manner without use of CMF substrate.

2.3. Materials characterization

The crystal structure of the obtained samples was characterized by XRD (Bruker D8 diffractometer) with CuK_α radiation ($\lambda = 0.1542$ nm) under a voltage of 40 kV and a current of 30 mA. The XPS analysis was performed on an ESCALab MKII X-ray photoelectron spectrometer using Mg Kα radiation. The microstructural properties of all samples were characterized using SEM (JEOL JSM-7001F) and TEM (Tecnai G2 20 TWIN TEM). The specific surface area and pore size distribution were characterized with a belsorp-max surface area detecting instrument (Tristar3000) by N_2 physisorption at 77 K.

2.4. Electrochemical measurements

The electrochemical HER tests of 3D CMF/$MoSe_2$ composite foams were performed in an electrolyte solution of 0.5 M H_2SO_4, respectively. A platinum wire and a saturated calomel electrode (SCE) were used as the counter electrode and the reference electrode, respectively. The working electrode was prepared by placing the free-standing CMF/$MoSe_2$ foam in an electrode clamp (Fig. S1), $MoSe_2$ and Pt/C electrodes were prepared by dropping 10 μL of $MoSe_2$ and Pt/C slurry (1 mg mL^{-1} in DI water) onto the polished glassy carbon electrode (GCE, 3 mm in diameter) and left to dry. All electrochemical studies were performed in a standard three-electrode setup using a CHI 660D electrochemical workstation (Shanghai Chenhua Instrument Co. China). Liner sweep voltammetry (LSV) measurements were conducted with a scan rate of 10 mV s^{-1}. The double-layer capacitance (C_{dl}) of the catalyst can be calculated from the cyclic voltammograms (CV) in the region of 0.1–0.2 V vs. RHE. By plotting Δj at 0.15 V vs. RHE against the scan rate, the slope is twice C_{dl}. In all measurements, the SCE reference electrode was calibrated with respect to the reversible hydrogen electrode (RHE) according to E (RHE) = E (SCE) + 0.059 pH V. The onset potential was determined based on the beginning of the linear region in the Tafel plot without iR compensation applied for all the electrochemical measurements. Electrochemical impedance spectroscopy (EIS) was recorded in the frequency ranging from 0.01 Hz to 100 kHz with an amplitude of 5 mV.

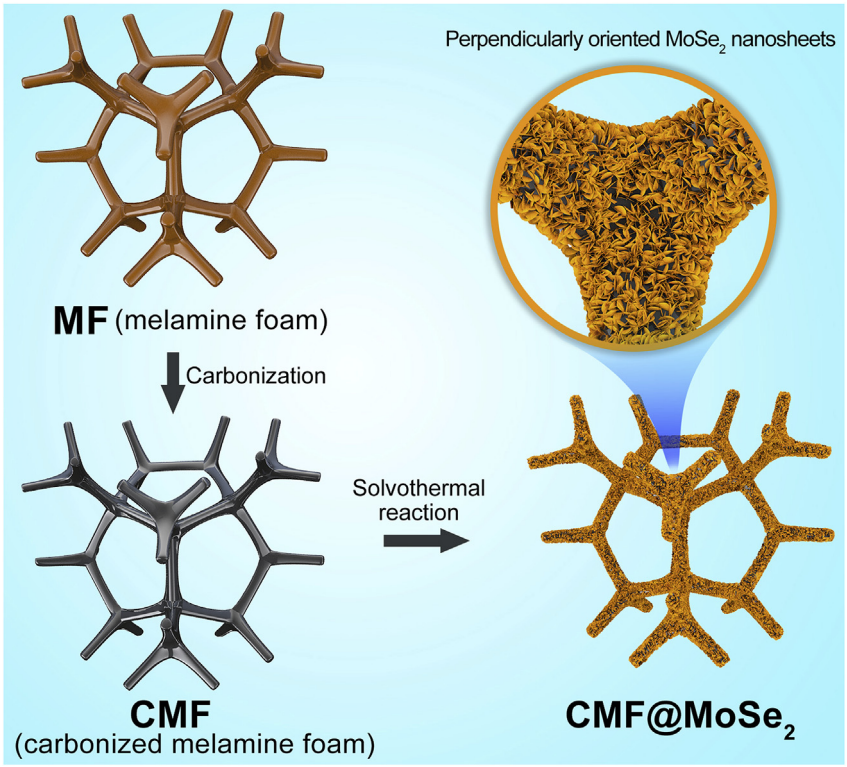

Scheme 1. Preparation procedure used to obtain the 3D CMF/$MoSe_2$ composite foam.

3. Results and discussion

MF was used in this work to prepare 3D carbon foam, which is mainly composed by formaldehyde-melamine resin, and is usually applied as abrasive cleaner and soundproofing materials. As presented in Fig. 1A, commercially available MF shows the well-defined 3D interconnected configuration with a concave triangle fiber shape. The CMF can be easily obtained through a direct carbonization of MF at 800 °C for 2 h in an inert atmosphere, where a great volume shrinkage occurred after the high-temperature treatment (Fig S2). In spite of the shape change, CMF almost inherits the 3D networks of MF. As shown in Fig. 1B, the interconnected architecture of CMF is composed by numerous cellular structures with pore diameters of about 50–70 nm. Due to high porosity of CMF (about 99.6%), it shows extremely lightweight with a density of about 5 mg cm^{-3}. Brunauer-Emmett-Teller (BET) analyses show the CMF has a high specific surface area of 178 $m^2 g^{-1}$ (Fig. S3A), the distribution of nano-sized pores in Fig. S3B may be attributed to the micro pores resulted from high temperature carbonization [47]. Additionally, the CMF also demonstrate excellent flexibility and resilience, which can endure a large scale bend and stretch deformation (Fig. S4). The structural robustness of CMF may originated from its firmly interconnected 3D carbon networks, which can withstand stress and load from all

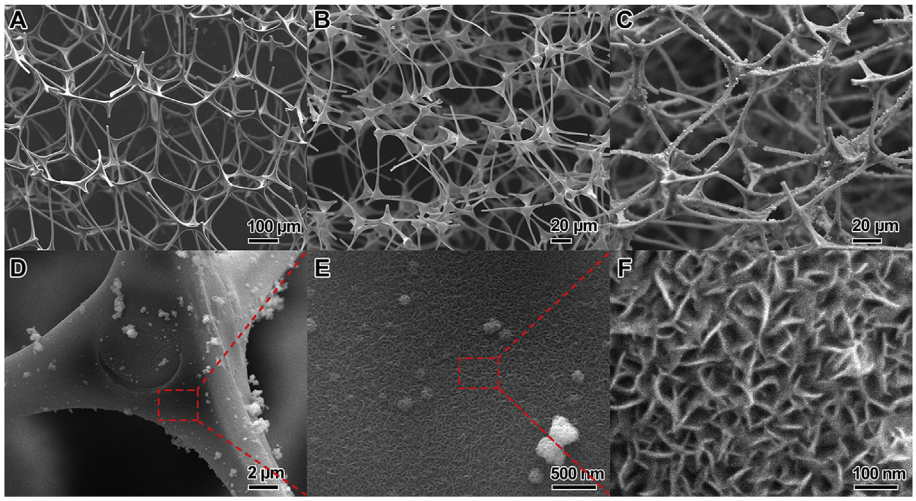

Fig. 1. SEM images of MF (A), CMF (B), and CMF/$MoSe_2$ composite foam at various magnifications (C-F).

directions. The excellent structure properties make CMF a perfect substrate for constructing 3D flexible electrodes.

Then, crystalized $MoSe_2$ nanosheets are deposited on CMF through a facile low-temperature solvothermal process combined with post annealing treatment. It can be observed from Fig. S5 that the structural stability and elasticity of the CMF substrate is well retained by the CMF/$MoSe_2$ composite foam. An overview in Fig. 1C and D presents the well-retained 3D macroporous networks of CMF/$MoSe_2$ composite foam, no large aggregations can be observed, indicating CMF is an applicable substrate for the growth of $MoSe_2$. A zoom-in view in Fig. 1E further reveals the uniform distribution of curled $MoSe_2$ subunits on CMF backbone. Under high-magnification, it can be clearly observed that $MoSe_2$ is grown with a sheet-like configuration and standing through a perpendicular orientation, which also intersect with each other to construct an open structure for electrolyte permeation. The unique combination of $MoSe_2$ nanosheets with 3D CMF frameworks can provide numerous exposed active edges and fast paths for charge transfer, which will potentially lead to an enhanced electrochemical activity of CMF/$MoSe_2$ composites. For comparison, pure $MoSe_2$ sample was also prepared in the absence of CMF substrate via the same method as CMF/$MoSe_2$ composites, which manifests an aggregated spherical structure with limited exposed $MoSe_2$ edges, further confirms the essential role of 3D CMF networks in mediating the uniform growth of $MoSe_2$ nanosheets. Fig. 2 presents the typical TEM images of CMF/$MoSe_2$ composite foam. It is obvious that $MoSe_2$ nanosheets are evenly distributed on the substrate with no large aggregation detected (Fig. 2A). TEM image under high magnification also reveals that individual $MoSe_2$ nanosheet in the composites is composed by 4–6 layers of $MoSe_2$ with the interlayer spacing of 0.65 nm (Fig. 2B), in accordance with the (002) lattice spacing of $MoSe_2$. It is worth mention that few-layered structure can further increase the density of exposed active edges of $MoSe_2$, thus potentially enhancing the electrochemical performance of CMF/$MoSe_2$ composites. The above morphological observations have given direct evidences on the successful growth of few-layered $MoSe_2$ nanosheets on 3D CMF frameworks.

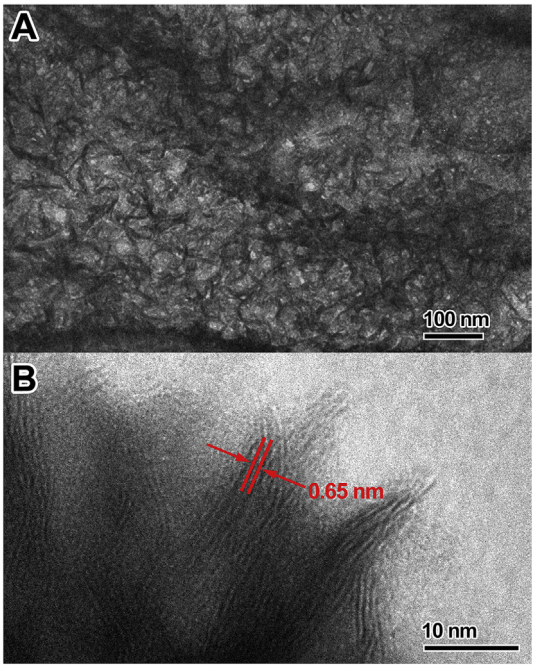

Fig. 2. TEM images of CMF/$MoSe_2$ composite foam at low (A) and high (B) magnifications.

The composition and crystal structure of CMF/$MoSe_2$ composites were studied by XRD as shown in Fig. 3. The peak located at $2\theta = 25^\circ$ in the curve of CMF is attributed to the amorphous structure of carbonaceous CMF. A series of diffraction peaks can be observed in the curve of CMF/$MoSe_2$ composites (i.e. $2\theta = 13.5^\circ$, 31.9°, 38.0°, and 56.2°), which can be readily indexed to the (002), (100), (103), and (110) diffraction planes of hexagonal 2H–$MoSe_2$ phase (JCPDF no. 87–2419), respectively. To further determine the oxidation state of $MoSe_2$ in CMF/$MoSe_2$ composites, XPS analysis was conducted with results shown in Fig. 4. Characteristic peaks of Mo, Se, and C elements can be clearly observed in the survey spectrum (Fig. 4A), matches well with the composition of CMF/$MoSe_2$ composites. Two peaks locate at 232.8 and 229.2 eV in the high-resolution spectrum of Mo 3d can be indexed to the Mo $3d_{3/2}$ and Mo $3d_{5/2}$ orbitals (Fig. 4B), indicating the Mo (IV) state of $MoSe_2$ in the composites. In addition, binding energies of Se $3d_{3/2}$ and Se $3d_{5/2}$ at 55.5 and 54.7 eV (Fig. 4C), along with Se $3p_{1/2}$ and Se $3p_{3/2}$ at 166.8 and 161.1 eV (Fig. 4D), all confirming the −2 oxidation chemical state of Se. Moreover, the detailed Mo:Se atomic ratio given by the compositional analysis is 9:20, in accordance with the formula of $MoSe_2$. All the structural characterizations further verify the successful synthesis of 3D hierarchical CMF/$MoSe_2$ foam.

3.1. HER performance of 3D CMF/$MoSe_2$ composite foam

The combination of electrical conductive 3D carbon networks with electrochemical active $MoSe_2$ nanosheets makes CMF/$MoSe_2$ composites extremely desirable for high-performance electrochemical applications. Since the 3D CMF/$MoSe_2$ composite foam possesses high structural stability and elasticity, it can be directly used as binder-free working electrode under the help of electrode clamp (Fig. S1). The electrochemical HER performance of CMF/$MoSe_2$ composite foam was investigated in 0.5 M H_2SO_4 solution using a typical three-electrode setup. Generally, an ideal HER catalyst is featured in low onset potential (the potential where HER activity starts), low Tafel slop comparable to that of Pt catalyst, as well as high current density at low overpotential.

To start with, comparison on the electrochemical activities of CMF/$MoSe_2$ composite, commercial Pt/C catalyst, physical mixture of CMF and $MoSe_2$ (denoted as CMF&$MoSe_2$), pure $MoSe_2$, and neat CMF electrodes was performed using LSV analyses. As shown in

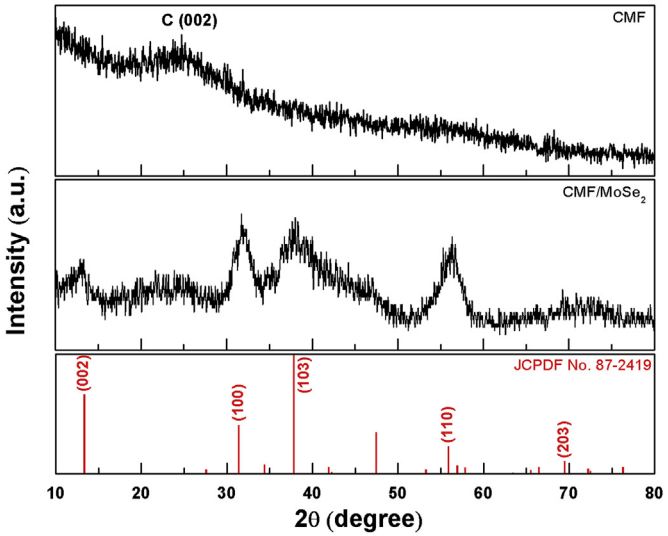

Fig. 3. XRD patterns of neat CMF, and CMF/$MoSe_2$ composite foam.

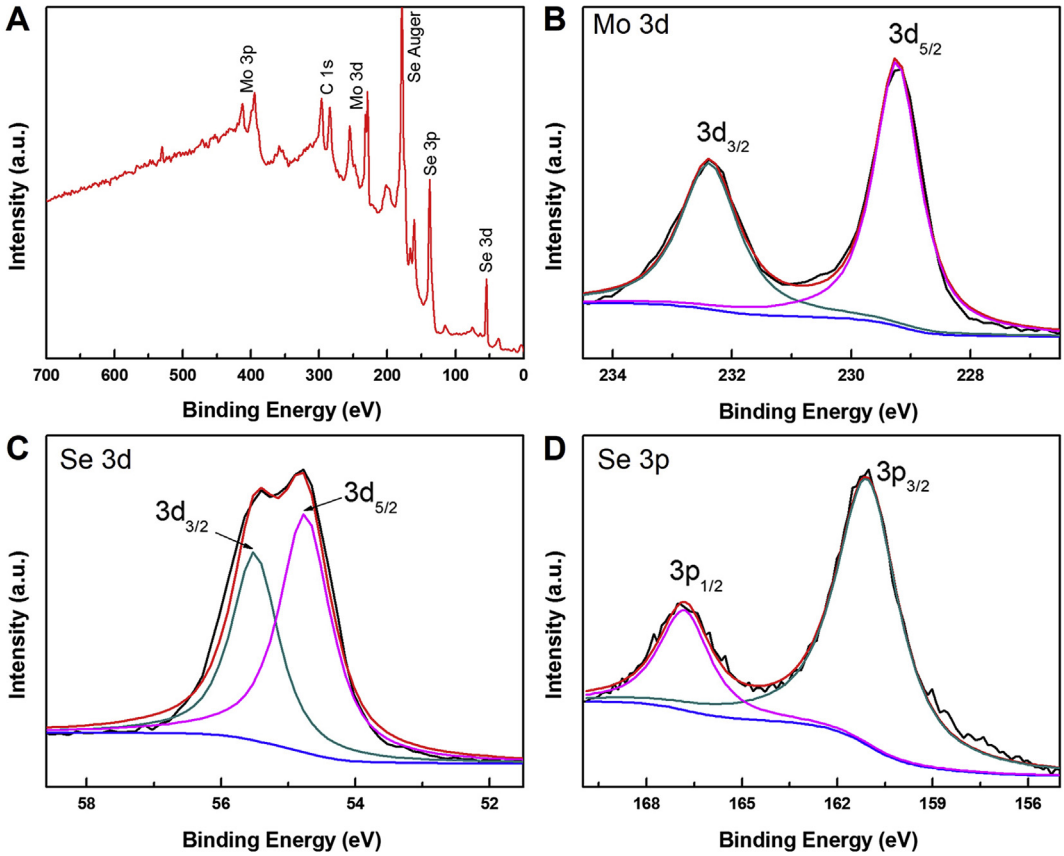

Fig. 4. XPS spectra of CMF/$MoSe_2$ composite foam: (A) survey spectrum, core-level spectra of (B) Mo 3d, (C) Se 3d and (D) Se 3p.

Fig. 5A, Pt/C modified electrode presents the best HER catalytic activity in terms of the smallest onset potential and the largest current density. On the contrary, neat CMF modified GCE shows no electrochemical activity with an almost horizontal line within the potential window. CMF&$MoSe_2$ and Pure $MoSe_2$ exhibit obvious electrochemical HER activity stemmed from the intrinsic electrochemical activity of LTMD, but still more negative onset potential and much lower anodic current compared with CMF/$MoSe_2$ composite electrode (−0.071 V vs. RHE). This may be caused by the rarity of available active sites of aggregated $MoSe_2$ spheres, and the absence of electrical coupling between CMF and $MoSe_2$, thus leading to the weak HER activity of CMF&$MoSe_2$ and Pure $MoSe_2$. The outperformed electrochemical HER activity of CMF/$MoSe_2$ composites (detailed comparison between different catalysts is provided in Table S1) reveals the successful design of the interconnected 3D catalyst, which incorporates the merits of 3D carbon networks and electro-active few-layered $MoSe_2$ in a reasonable manner to achieve synergistically enhanced HER performance.

The Tafel slope, which can be obtained from Tafel equation ($\eta = b\ \log(j) + a$, where η is the overpotential, b is the Tafel slope and j is the current density) based on the corresponding LSV curves of electrodes, is correlated with the reaction pathway and adsorption type of HER catalysts, and usually represents the inherent electrocatalytic property determined by the rate limiting steps of HER. Fig. 5B presents the Tafel plots of different electrodes, which gives the Tafel slop of about 78.6, 49.3, and 33.1 mV dec^{-1} for pure $MoSe_2$, CMF/$MoSe_2$ composites, and Pt/C catalysts, respectively. The smaller Tafel slope of CMF/$MoSe_2$ composites than that of pure $MoSe_2$ implies the faster increament of HER rate with increasing overpotential, which is important in the practical applications. Additionally, with a Tafel slope of 49.3 mV dec^{-1}, the HER process of CMF/$MoSe_2$ composite catalyst can be assigned as the Volmer-Heyrovsky or the Volmer-Tafel mechanism with the Volmer reaction as the rate-determine step. On the other hand, electrochemical double-layer capacitance (C_{dl}) measurement was carried out using cyclic voltammetry (CV) tests to estimate the effective surface area of the solid-liquid interface [48]. As shown in Fig. 5C and D, the CMF/$MoSe_2$ composite foam display the biggish C_{dl} of about 25.1 mF cm^{-2}, demonstrating there was more active sites involved in the electrochemical process, thus resulting in the excellent HER performance of CMF/$MoSe_2$ composite foam.

In order to investigate the electrochemical behavior of the electrodes during HER testing environments, electrochemical impedance spectroscopy (EIS) analyses were performed on neat CMF, pure $MoSe_2$, and CMF/$MoSe_2$ composites electrodes. As can be observed from Fig. 6, typically, the visible semicircles in the low frequency range of Nyquist plots are mainly ascribed to the charge transfer resistance (R_{ct}) of H^+ reduction at the electrode-electrolyte interface, the x-intercept of Nyquist plots are normally stemmed from the series resistance (R_s) of the catalysts. It is obvious that R_{ct} of CMF/$MoSe_2$ composites is greatly decreased than that of pure $MoSe_2$, indicating that.

CMF with larger surface area and 3D interconnected architecture can mediate the uniform distribution of few-layered $MoSe_2$ nanosheets, thus significantly enhance the charge transfer efficiency along the electrode-electrolyte interface. additionally, CMF/$MoSe_2$ composite foam also reveals smaller R_s compared with pure $MoSe_2$ nanospheres, implying the intimate coupling between few-layered $MoSe_2$ nanosheets and electrical conductive CMF frameworks can offer fast routs for efficient electron transfer. These EIS

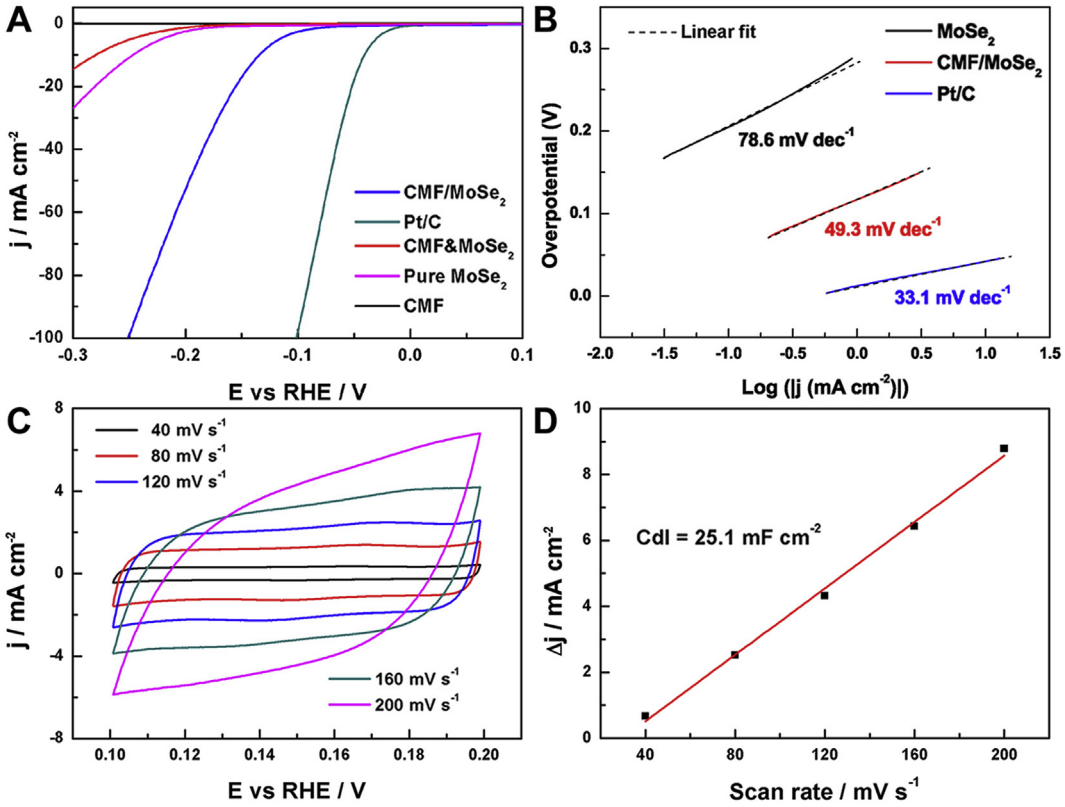

Fig. 5. LSV polarization curves for different electrodes in N_2-purged 0.5 M H_2SO_4 solution. Scan rate: 5 mV s^{-1} (A). Tafel plots for pure $MoSe_2$, Pt/C, and CMF/$MoSe_2$ electrodes (B). CV curves of the CMF/$MoSe_2$ composite electrode at different scan rates in the region of 0.1–0.2 V vs. RHE (C). Plot showing the extraction of the double layer capacitance (C_{dl}) for the CMF/$MoSe_2$ composite electrode at 0.15 V (D).

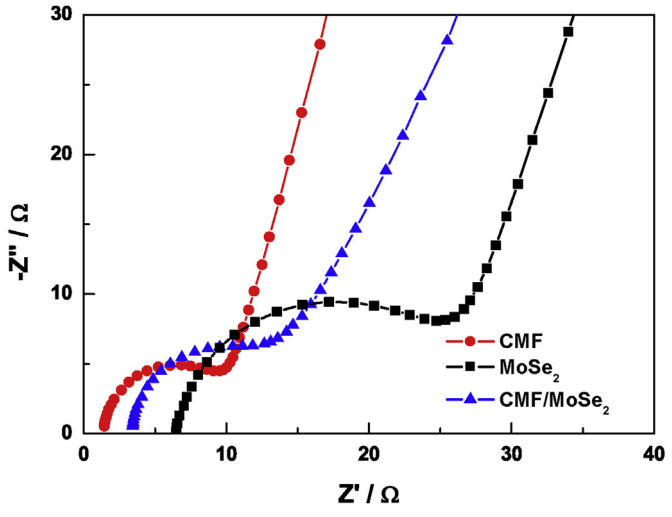

Fig. 6. Nyquist plots for neat CMF, pure $MoSe_2$ nanosheets, and CMF/$MoSe_2$ composite foam.

results further highlight the successful design of the 3D hierarchical CMF/$MoSe_2$ composite foam as high-performance Pt-free HER catalyst. Long-cycle durability is of vital significance for a HER catalyst in industrial applications. Here, the LSV curves of CMF/$MoSe_2$ composite before and after 3000 cyclic voltammetry (CV, from −0.3 V to 0.1 V (vs. RHE) at 100 mV s^{-1}) cycles is shown in Fig. 7A. It is evident that CMF/$MoSe_2$ composite retains almost the same low HER onset potential, but with a slight decline on the current density, indicating the good stability of the CMF/$MoSe_2$ composite catalyst. The current decay may be caused by the gradual accumulation of $MoSe_2$ nanosheets (Fig. 7B), thus slightly decrease the number of exposed active edges for HER process.

The electrochemical HER process is intrinsically an interfacial reaction involving the adsorption and dissociation of hyfrogen molecules mainly on the surface/interface of the catalysts, that means more accessible electro-active sites and high ion/charge transfer efficiency potentially lead to better HER performance. Based on this concept, the remarkable HER capability of CMF/$MoSe_2$ composite foam is assumed to be attributed to the hierarchical few-layered $MoSe_2$ nanosheets backboned with 3D interconnected carbon networks (Scheme 2), which can be summarized into three aspects. To begin with, 3D CMF frameworks with excellent porocity could provide substantial nucleation sites for the uniform distribution of $MoSe_2$ nanosheets. Secondly, deposited few-layered $MoSe_2$ nanosheets with fully exposed active edges and open structures could offer numerous active sites to facilitate efficient HER process. Lastly, the heterogeneous architecture of CMF/$MoSe_2$ composite foam could ensure fast charge transport kinetics benefiting from the electrical conductive 3D interconnected CMF networks. The integration of above three factors gives birth to the 3D hierarchical CMF/$MoSe_2$ composite foam with excellent HER catalytic capability.

4. Conclusions

In summary, we have demonstrated a versatile paradigm for the fabrication of 3D flexible catalyst by depositing electrochemical active $MoSe_2$ nanosheets on elastic CMF for high-performance electrochemical HER. The efficient two-step synthesis involves

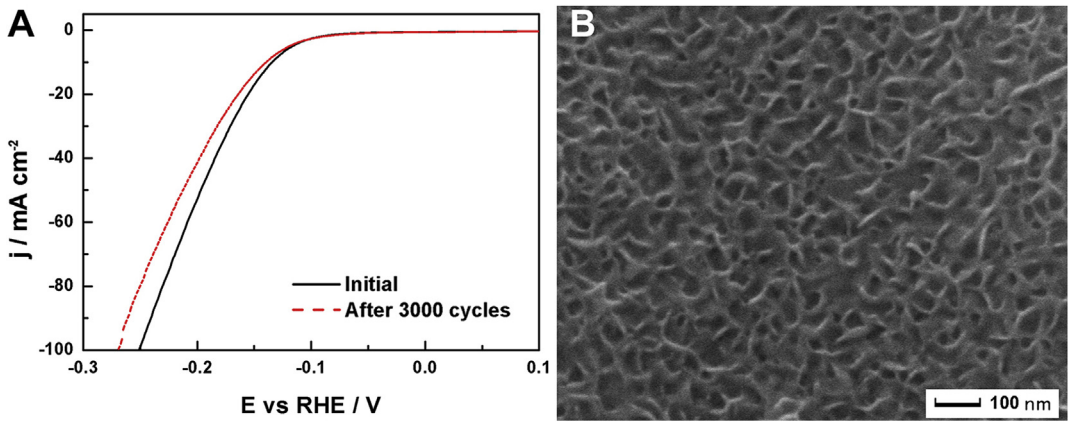

Fig. 7. LSV polarization curves for CMF/$MoSe_2$ composite electrode recorded before and after 3000 times of CV cycles (A), and SEM image of CMF/$MoSe_2$ composite foam after cycling test (B).

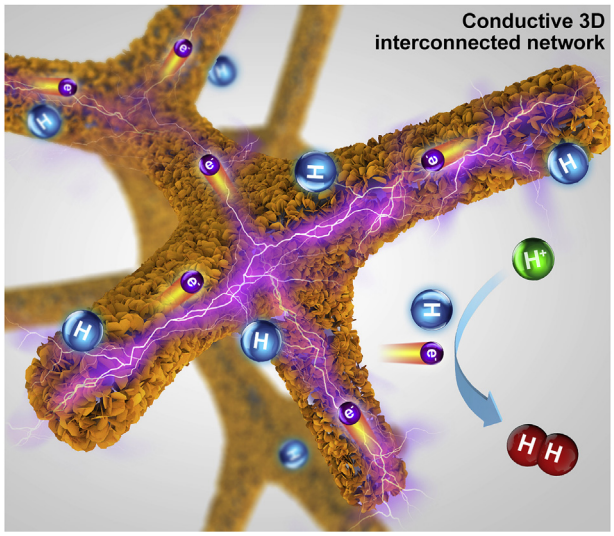

Scheme 2. Schematic representation of fast charge transfer and efficient ion diffusion during the HER process of CMF/$MoSe_2$ composite foam.

the direct carbonization of polymeric MF and subsequent growth of few-layered $MoSe_2$ nanosheets through a simple solvothermal reaction. This rationally designed interconnected 3D architecture not only realizes the uniform deposition of $MoSe_2$ nanosheets, but also affords efficient and rapid pathways for ion and electron transport through the carbonaceous backbone and the intimate interaction between two components. Thus resulted flexible and lightweight CMF/$MoSe_2$ composite foam with fully exposed active edges exhibit greatly improved electrochemical HER catalytic activity featured in a low onset potential of −0.071 V vs. RHE and small Tafel slope of 49.3 mV dec^{-1}. The presented encouraging results open up the possibility for the development of 3D flexible catalysts for high-performance HER.

Acknowledgements

This work is financially supported by the National Natural Science Foundation of China for Youths (No.21704035), the China Postdoctoral Science Foundation (Nos. 2017M610304), Natural Science Foundation of Jiangsu Province for Youths (BK20170544), University Natural Science Research of Jiangsu (No.17KJB430010), Jiangsu Province Postdoctoral Science Foundation (1701065C), and a Project Funded by the Priority Academic Program Development of Jiangsu Higher Education Institutions.

Appendix A. Supplementary data

Supplementary data related to this article can be found at https://doi.org/10.1016/j.electacta.2018.01.016.

References

[1] K.Z. Cao, H.Q. Liu, Y. Li, Y.J. Wang, L.F. Jiao, Encapsulating sulfur in δ-MnO_2 at room temperature for Li-S battery cathode, Energy Storage Mater (2017) 78–84.
[2] Z.M. Liu, T.C. Lu, T. Song, X.Y. Yu, X.W.D. Lou, U. Paik, Structure-designed synthesis of FeS_2@C yolk-shell nanoboxes as a high-performance anode for sodium-ion batteries, Energy Environ. Sci. (2017) 1576–1580.
[3] J. Zhang, T. Wang, P. Liu, Z.Q. Liao, S.H. Liu, X.D. Zhuang, M.W. Chen, E. Zschech, X.L. Feng, Efficient hydrogen production on $MoNi_4$ electrocatalysts with fast water dissociation kinetics, Nat. Commun. (2017) 15437.
[4] Y. Zhao, M. Yuan, Y. Chen, J. Yan, L. Xu, Y.P. Huang, J.B. Lian, J. Bao, J.X. Qiu, L. Xu, Y.G. Xu, H. Xu, H.M. Li, Construction of molybdenum dioxide nanosheets coated on the surface of nickel ferrite nanocrystals with ultrahigh specific capacity for hybrid supercapacitor, Electrochim. Acta (2017), https://doi.org/10.1016/j.electacta.2017.12.053.
[5] J. Turner, G. Sverdrup, M.K. Mann, P. Maness, B. Kroposki, M. Ghirardi, R.J. Evans, D. Blake, Renewable hydrogen production, Int. J. Energy Res. 5 (2008) 379–407.
[6] S. Dunn, Hydrogen futures: toward a sustainable energy system, Int. J. Hydrogen Energy 3 (2002) 235–264.
[7] T. Tang, W.J. Jiang, S. Niu, N. Liu, H. Luo, Y.Y. Chen, S.F. Jin, F. Gao, L.J. Wan, J.S. Hu, Electronic and morphological dual modulation of cobalt carbonate hydroxides by Mn doping toward highly efficient and stable bifunctional electrocatalysts for overall water splitting, J. Am. Chem. Soc. (2017) 8320–8328.
[8] D.Y. Chung, S.W. Jun, G. Yoon, H. Kim, J.M. Yoo, K. Lee, T. Kim, H. Shin, A.K. Sinha, S.G. Kwon, K. Kang, T. Hyeon, Y. Sung, Large-scale synthesis of carbon-shell-coated FeP nanoparticles for robust hydrogen evolution reaction electrocatalyst, J. Am. Chem. Soc. (2017) 6669–6674.
[9] Y.T. Xu, X.F. Xiao, Z.M. Ye, S.L. Zhao, R.A. Shen, C.T. He, J.P. Zhang, Y.D. Li, X.M. Chen, Cage-confinement pyrolysis route to ultrasmall tungsten carbide nanoparticles for efficient electrocatalytic hydrogen evolution, J. Am. Chem. Soc. 15 (2017) 5285–5288.
[10] M. Caban-Acevedo, M.L. Stone, J.R. Schmidt, J.G. Thomas, Q. Ding, H. Chang, M. Tsai, J. He, S. Jin, Efficient hydrogen evolution catalysis using ternary pyrite-type cobalt phosphosulphide, Nat. Mater. 12 (2015) 1245–1251.
[11] J. Kibsgaard, T.F. Jaramillo, Molybdenum phosphosulfide: an active, acid-stable, earth-abundant catalyst for the hydrogen evolution reaction, Angew. Chem. Int. Ed. 52 (2014) 14433–14437.
[12] J. Staszak-Jirkovsky, C.D. Malliakas, P.P. Lopes, N. Danilovic, S.S. Kota, K. Chang, B. Genorio, D. Strmcnik, V.R. Stamenkovic, M.G. Kanatzidis, N.M. Markovic, Design of active and stable Co-Mo-S_x chalcogels as pH-universal catalysts for the hydrogen evolution reaction, Nat. Mater. 2 (2016) 197–203.
[13] X. Zhao, X. Ma, J. Sun, D.H. Li, X.R. Yang, Enhanced catalytic activities of surfactant-assisted exfoliated WS_2 nanodots for hydrogen evolution, ACS Nano 2 (2016) 2159–2166.
[14] M.A. Lukowski, A.S. Daniel, F. Meng, A. Forticaux, L.S. Li, S. Jin, Enhanced

hydrogen evolution catalysis from chemically exfoliated metallic MoS_2 nanosheets, J. Am. Chem. Soc. 28 (2013) 10274–10277.
[15] H.T. Wang, H. Lee, Y. Deng, Z.Y. Lu, P. Hsu, Y.Y. Liu, D.C. Lin, Y. Cui, Bifunctional non-noble metal oxide nanoparticle electrocatalysts through lithium-induced conversion for overall water splitting, Nat. Commun. (2015) 7261.
[16] J.X. Feng, L.X. Ding, S.H. Ye, X.J. He, H. Xu, Y.X. Tong, G.R. Li, $Co(OH)_2$@PANI hybrid nanosheets with 3D networks as high-performance electrocatalysts for hydrogen evolution reaction, Adv. Mater. 44 (2015) 7051–7057.
[17] N. Danilovic, R. Subbaraman, D. Strmcnik, K.C. Chang, A.P. Paulikas, V.R. Stamenkovic, N.M. Markovic, Enhancing the alkaline hydrogen evolution reaction activity through the bifunctionality of $Ni(OH)_2$/metal catalysts, Angew. Chem. Int. Ed. 50 (2012) 12663–12666.
[18] C. Tang, R. Zhang, W.B. Lu, L.B. He, X. Jiang, A.M. Asiri, X.P. Sun, Fe-doped CoP nanoarray: a monolithic multifunctional catalyst for highly efficient hydrogen generation, Adv. Mater. 2 (2017) 1602441.
[19] Z.C. Xing, Q. Liu, A.M. Asiri, X.P. Sun, Closely interconnected network of molybdenum phosphide nanoparticles: a highly efficient electrocatalyst for generating hydrogen from water, Adv. Mater. 32 (2014) 5702–5707.
[20] E.J. Popczun, J.R. McKone, C.G. Read, A.J. Biacchi, A.M. Wiltrout, N.S. Lewis, R.E. Schaak, Nanostructured nickel phosphide as an electrocatalyst for the hydrogen evolution reaction, J. Am. Chem. Soc. 25 (2013) 9267–9270.
[21] Y.Q. Zhang, B. Ouyang, J. Xu, S. Chen, R.S. Rawat, H.J. Fan, 3D porous hierarchical nickel-molybdenum nitrides synthesized by RF plasma as highly active and stable hydrogen-evolution-reaction electrocatalysts, Adv. Energy Mater 11 (2016), 1600221.
[22] W.F. Chen, K. Sasaki, C. Ma, A.I. Frenkel, N. Marinkovic, J.T. Muckerman, Y.M. Zhu, R.R. Adzic, Hydrogen-evolution catalysts based on non-noble metal nickel-molybdenum nitride nanosheets, Angew. Chem. Int. Ed. 25 (2012) 6131–6135.
[23] H. Vrubel, X.L. Hu, Molybdenum boride and carbide catalyze hydrogen evolution in both acidic and basic solutions, Angew. Chem. Int. Ed. 51 (2012) 12875–12878.
[24] L. Liao, S.N. Wang, J.J. Xiao, X.J. Bian, Y.H. Zhang, M.D. Scanlon, X.L. Hu, Y. Tang, B.H. Liu, H.H. Girault, A nanoporous molybdenum carbide nanowire as an electrocatalyst for hydrogen evolution reaction, Energy Environ. Sci. 1 (2014) 387–392.
[25] J. Lin, Z.W. Peng, G. Wang, D. Zakhidov, E. Larios, M.J. Yacaman, J.M. Tour, Enhanced electrocatalysis for hydrogen evolution reactions from WS_2 nanoribbons, Adv. Energy Mater 10 (2014) 1301875.
[26] Y. Yang, H.L. Fei, G.D. Ruan, C.S. Xiang, J.M. Tour, Edge-oriented MoS2 nanoporous films as flexible electrodes for hydrogen evolution reactions and supercapacitor devices, Adv. Mater. 48 (2014) 8163–8168.
[27] X.L. Zhou, J. Jiang, T. Ding, J.J. Zhang, B.C. Pan, J. Zuo, Q. Yang, Fast colloidal synthesis of scalable Mo-rich hierarchical ultrathin MoSe, Nanoscale 19 (2014) 11046–11051.
[28] Y.F. Shi, C.X. Hua, B. Li, X.P. Fang, C.H. Yao, Y.C. Zhang, Y.S. Hu, Z.X. Wang, L.Q. Chen, D.Y. Zhao, G.D. Stucky, Highly ordered mesoporous crystalline $MoSe_2$ material with efficient visible-light-driven photocatalytic activity and enhanced lithium storage performance, Adv. Funct. Mater. 14 (2013) 1832–1838.
[29] C. Xu, S.J. Peng, C.L. Tan, H.X. Ang, H.T. Tan, H. Zhang, Q.Y. Yan, Ultrathin S-doped $MoSe_2$ nanosheets for efficient hydrogen evolution, J. Mater. Chem. A 16 (2014) 5597–5601.
[30] H. Tang, K.P. Dou, C.C. Kaun, Q. Kuang, S.H. Yang, $MoSe_2$ nanosheets and their graphene hybrids: synthesis, characterization and hydrogen evolution reaction studies, J. Mater. Chem. A 2 (2014) 360–364.
[31] S.J. Deng, Y. Zhong, Y.X. Zeng, Y.D. Wang, Z.J. Yao, F. Yang, S.W. Lin, X.L. Wang, X.H. Lu, X.H. Xia, J.P. Tu, Directional construction of vertical nitrogen-doped 1T-2H $MoSe_2$/graphene shell/core nanoflake arrays for efficient hydrogen evolution reaction, Adv. Mater. (2017) 1700748.
[32] L.P. Jia, X. Sun, Y.M. Jiang, S.J. Yu, C.M. Wang, A novel $MoSe_2$-reduced graphene oxide/polyimide composite film for applications in electrocatalysis and photoelectrocatalysis hydrogen evolution, Adv. Funct. Mater. 12 (2015) 1814–1820.
[33] S. Mao, Z.H. Wen, S.Q. Ci, X.R. Guo, K.K. Ostrikov, J.H. Chen, Perpendicularly oriented $MoSe_2$/graphene nanosheets as advanced electrocatalysts for hydrogen evolution, Small 4 (2015) 414–419.
[34] Y.P. Huang, Y.E. Miao, J. Fu, S.Y. Mo, C. Wei, T.X. Liu, Perpendicularly oriented few-layer $MoSe_2$ on SnO_2 nanotubes for efficient hydrogen evolution reaction, J. Mater. Chem. A 31 (2015) 16263–16271.
[35] B. Qu, X.B. Yu, Y.J. Chen, C.L. Zhu, C.Y. Li, Z.X. Yin, X.T. Zhang, Ultrathin $MoSe_2$ nanosheets decorated on carbon fiber cloth as binder-free and high-performance electrocatalyst for hydrogen evolution, ACS Appl. Mater. Interfaces 26 (2015) 14170–14175.
[36] H.J. Chen, Y. Xie, H.L. Cui, W. Zhao, X.L. Zhu, Y.M. Wang, X.J. Lu, F.Q. Huang, In situ growth of a $MoSe_2$/Mo counter electrode for high efficiency dye-sensitized solar cells, Chem. Commun. 34 (2014) 4475–4477.
[37] C. Zhu, T.Y. Han, E.B. Duoss, A.M. Golobic, J.D. Kuntz, C.M. Spadaccini, M.A. Worsley, Highly compressible 3D periodic graphene aerogel microlattices, Nat. Commun. (2015) 6962.
[38] Y. Zhao, J. Liu, Y. Hu, H.H. Cheng, C.G. Hu, C.C. Jiang, L. Jiang, A.Y. Cao, L.T. Qu, Highly compression-tolerant supercapacitor based on polypyrrole-mediated graphene foam electrodes, Adv. Mater. 4 (2013) 591–595.
[39] L. Li, K. Wang, Z.Q. Huang, C. Zhang, T.X. Liu, Highly ordered graphene architectures by duplicating melamine sponges as a three-dimensional deformation-tolerant electrode, Nano Res. 10 (2016) 2938–2949.
[40] H. Im, T. Kim, H. Song, J. Choi, J.S. Park, R. Ovalle-Robles, H.D. Yang, K.D. Kihm, R.H. Baughman, H.H. Lee, T.J. Kang, Y.H. Kim, High-efficiency electrochemical thermal energy harvester using carbon nanotube aerogel sheet electrodes, Nat. Commun. (2016) 10600.
[41] J.H. Kim, S.T. Myung, Y.K. Sun, Molten salt synthesis of $LiNi_{0.5}Mn_{1.5}O_4$ spinel for 5 V class cathode material of Li-ion secondary battery, Electrochim. Acta 2 (2004) 219–227.
[42] S.H. Yan, X. Zhen, G. Chao, Multifunctional, ultra-flyweight, synergistically assembled carbon aerogels, Adv. Mater. (2013) 2554–2560.
[43] Y. Qin, J. Yuan, J. Li, D.C. Chen, Y. Kong, F.Q. Chu, Y.X. Tao, M.L. Liu, Crosslinking graphene oxide into robust 3D porous N-doped graphene, Adv. Mater. 35 (2015) 5171–5175.
[44] L.F. Shen, J. Wang, G.Y. Xu, H.S. Li, H. Dou, X.G. Zhang, $NiCo_2S_4$ nanosheets grown on nitrogen-doped carbon foams as an advanced electrode for supercapacitors, Adv. Energy Mater 3 (2015) 1400977.
[45] K. Xiao, L.X. Ding, G.X. Liu, H.B. Chen, S.Q. Wang, H.H. Wang, Freestanding, hydrophilic nitrogen-doped carbon foams for highly compressible all solid-state supercapacitors, Adv. Mater. 28 (2016) 5997–6002.
[46] S.L. Chen, G.H. He, H. Hu, S.Q. Jin, Y. Zhou, Y.Y. He, S.J. He, F. Zhao, H.Q. Hou, Elastic carbon foam via direct carbonization of polymer foam for flexible electrodes and organic chemical absorption, Energy Environ. Sci. 8 (2013) 2435–2439.
[47] H. Zhang, Y. Zhou, C.G. Li, S.L. Chen, L. Liu, S.W. Liu, H.M. Yao, H.Q. Hou, Porous nitrogen doped carbon foam with excellent resilience for self-supported oxygen reduction catalyst, Carbon 95 (2015) 388–395.
[48] R.G. Ma, Y. Zhou, Y.F. Chen, P.X. Li, Q. Liu, J.C. Wang, Ultrafine molybdenum carbide nanoparticles composited with carbon as a highly active hydrogen-evolution electrocatalyst, Angew. Chem. Int. Ed. 49 (2015) 14723–14727.